Light trapping in solar cells: numerical modeling with measured surface textures

Thomas Lanz,[1,4] **Kevin Lapagna,**[1] **Stéphane Altazin,**[2] **Mathieu Boccard,**[3] **Franz-Josef Haug,**[3] **Christophe Ballif,**[3] **and Beat Ruhstaller**[1,2,*]

[1]*Zurich University of Applied Sciences, School of Engineering, Institute of Computational Physics, Wildbachstrasse 21, CH-8401 Winterthur, Switzerland*
[2]*Fluxim AG, Technoparkstrasse 2, 8406 Winterthur, Switzerland*
[3]*Ecole Polytechnique Fédérale de Lausanne, Institute of Microengineering, Photovoltaics and Thin Film Electronics Laboratory, MC A2 304 (Microcity), Rue de la Maladière 71, CH-2000 Neuchâtel, Switzerland*
[4]*thomas.lanz@umu.se*
[*]*beat.ruhstaller@zhaw.ch*

Abstract: We present and experimentally validate a computational model for the light propagation in thin-film solar cells that integrates non-paraxial scalar diffraction theory with non-sequential ray-tracing. The model allows computing the spectral layer absorbances of solar cells with micro- and nano-textured interfaces directly from measured surface topographies. We can thus quantify decisive quantities such as the parasitic absorption without relying on heuristic scattering intensity distributions. In particular, we find that the commonly used approximation of Lambertian scattering intensity distributions for internal light propagation is violated even for solar cells on rough textured substrates. More importantly, we demonstrate how both scattering and parasitic absorption must be controlled to maximize photocurrent.

© 2015 Optical Society of America

OCIS codes: (290.5880) Scattering, rough surfaces; (080.1753) Computation methods; (070.7345) Wave propagation; (310.6805) Theory and design; (040.5350) Photovoltaic.

References and links

1. International Energy Agency, “Tracking clean energy progress 2014,” `http://www.iea.org/publications/freepublications/publication/tracking-clean-energy-progress-2014.html`.
2. P. Kowalczewski, M. Liscidini, and L. C. Andreani, “Engineering gaussian disorder at rough interfaces for light trapping in thin-film solar cells,” Opt. Lett. **37**, 4868–4870 (2012).
3. A. Bozzola, M. Liscidini, and L. C. Andreani, “Photonic light-trapping versus lambertian limits in thin film silicon solar cells with 1D and 2D periodic patterns,” Opt. Express **20**, A224–A244 (2012).
4. T. Lanz, L. Fang, S. Baik, K. Lim, and B. Ruhstaller, “Photocurrent increase in amorphous Si solar cells by increased reflectivity of LiF/Al electrodes,” Sol. Energ. Mat. Sol. Cells **107**, 259–262 (2012).
5. A. Bozzola, P. Kowalczewski, and L. C. Andreani, “Towards high efficiency thin-film crystalline silicon solar cells: The roles of light trapping and non-radiative recombinations,” J. Appl. Phys. **115**, 094501 (2014).
6. K. Jager, M. Fischer, R. A. C. M. M. van Swaaij, and M. Zeman, “A scattering model for nano-textured interfaces and its application in opto-electrical simulations of thin-film silicon solar cells,” J. Appl. Phys. **111**, 083108 (2012).
7. M. Boccard, C. Battaglia, F.-J. Haug, M. Despeisse, and C. Ballif, “Light trapping in solar cells: Analytical modeling,” Appl. Phys. Lett. **101**, 151105 (2012).
8. E. Yablonovitch, “Statistical ray optics,” J. Opt. Soc. Am. A **72**, 899–907 (1982).
9. H. Zhao, B. Ozturk, E. Schiff, L. Sivec, B. Yan, J. Yang, and S. Guha, “Backreflector morphology effects and thermodynamic light-trapping in thin-film silicon solar cells,” Sol. Energ. Mat. Sol. Cells **129**, 104–114 (2014).

#233350 - $15.00 USD Received 6 Feb 2015; revised 17 Mar 2015; accepted 18 Mar 2015; published 17 Apr 2015
(C) 2015 OSA 1 June 2015 | Vol. 23, No. 11 | DOI:10.1364/OE.22.00A539 | OPTICS EXPRESS A540

10. C. Battaglia, M. Boccard, F.-J. Haug, and C. Ballif, “Light trapping in solar cells: When does a Lambertian scatterer scatter Lambertianly?” J. Appl. Phys. **112**, 094504 (2012).
11. C. S. Schuster, A. Bozzola, L. C. Andreani, and T. F. Krauss, “How to assess light trapping structures versus a lambertian scatterer for solar cells?” Opt. Express **22**, A542–A551 (2014).
12. T. Lanz, B. Ruhstaller, C. Battaglia, and C. Ballif, “Extended light scattering model incorporating coherence for thin-film silicon solar cells,” J. Appl. Phys. **110**, 033111 (2011).
13. J. E. Harvey, C. L. Vernold, A. Krywonos, and P. L. Thompson, “Diffracted radiance: A fundamental quantity in nonparaxial scalar diffraction theory,” Appl. Opt. **38**, 6469–6481 (1999).
14. D. Domine, F. J. Haug, C. Battaglia, and C. Ballif, “Modeling of light scattering from micro- and nanotextured surfaces,” J. Appl. Phys. **107**, 044504 (2010).
15. J. E. Harvey, A. Krywonos, and D. Bogunovic, “Nonparaxial scalar treatment of sinusoidal phase gratings,” J. Opt. Soc. Am. A **23**, 858–865 (2006).
16. A. V. Gitin, “Huygens-Feynman-Fresnel principle as the basis of applied optics,” Appl. Opt. **52**, 7419–7434 (2013).
17. Fluxim Inc., www.fluxim.com.
18. S. Altazin, K. Lapagna, T. Lanz, C. Kirsch, R. Knaack, and B. Ruhstaller, “40.4: Design tool for light scattering enhancement in OLEDs,” SID Int. Symp. Dig. Tec. **45**, 576–579 (2014).
19. D. Dominé, “The role of front electrodes and intermediate reflectors in the optoelectronic properties of high-efficiency micromorph solar cells,” Ph.D. thesis, Université de Neuchâtel (2009).
20. B. T. Phong, “Illumination for computer generated pictures,” Commun. ACM **18**, 311–317 (1975).

1. Introduction

Harvesting of renewable energy is by now widely accepted to be able to contribute significantly to a sustainable future energy mix. Renewable power generation grew by 5.5% annually in the years from 2006 to 2013 and is expected to grow even faster in the near future. Among the different technologies, the installed capacity of solar photovoltaics (PV) alone grew by 37% in 2013 [1]. Further growth for solar PV can be facilitated by improving the price/performance ratio. One promising route for thin-film solar technologies is by improving the light trapping: to maximise the harvesting of the incident radiation. Our contribution aims to support this endeavour by presenting an accurate and efficient numerical model of the light propagation that allows testing of real surface textures for their suitability as textured interfaces in solar cells.

To optically model high-efficiency thin-film solar cells requires tackling both the micro- and nano-textured interfaces used to achieve light trapping, as well as the large width to height aspect ratio of these devices. Among the several methods that have been used to address this problem are RCWA [2, 3], transfer matrix formalism [4, 5], scalar scattering theories [6, 7] as well as analytical approaches based on statistical ray optics [8, 9]. The latter rely on calculating the absorption by tracing an average ray of light through the structure. By assuming full randomization of the internally scattered light this approach allows deriving an absorption enhancement factor of $4n^2$ for weak absorption, where n is the refractive index. Full randomization of the radiation is characterized by constant radiance which corresponds to a Lambertian intensity distribution (i.e. proportional to the cosine of the observation angle, independent of the incidence angle). Recently, two terms have been introduced to quantify the comparison of a scattering structure to a Lambertian scatterer: the Lambertionality factor [10] and the light trapping efficiency [11]. These concepts provide figures of merit to assess light trapping in comparison to the benchmark of Lambertian scattering. Contrastingly, our model assesses the light trapping ability of differently textured interfaces by computing the light propagation within the structures containing these interfaces. In contrast to earlier presented approaches we do not rely on assumptions about the intensity distributions of secondary and higher scattering events.

We extend our earlier model that integrates thin-film optics with non-iterative ray-tracing [12] with an interface model that relies on non-paraxial scalar scattering theory [13, 14]. We demonstrate that this interface model correctly describes the scattering at nano-textured interfaces even for oblique incidence, which is a prerequisite for avoiding heuristic scattering intensity distributions.

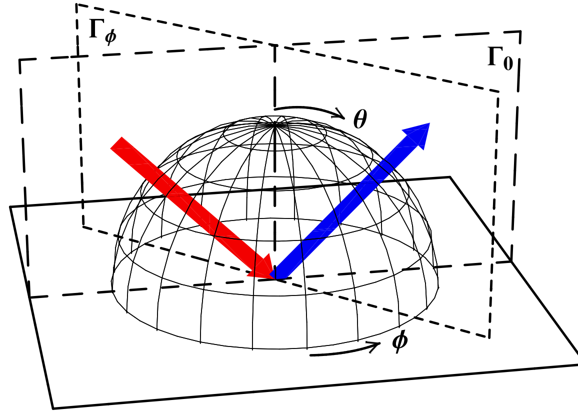

Fig. 1. Illustration for the case of reflection: the plane of incidence Γ_0, a plane Γ_ϕ, the hemisphere and its coordinates on which the angle resolved scattering (ARS) is defined. The red arrow illustrates oblique incidence, the blue arrow the specular part of the reflected light.

2. Methods

Our earlier developed absorption model computes the spectral absorption profiles by means of non-iterative ray-tracing [12]. We integrate over all azimuth angles and thus represent the propagating radiation by the discretized polar angle only. This restricts our method to interface textures that are azimuthally symmetric in a statistical sense. The fluxes in the various layers are connected by (specular or diffuse) transmission and reflection at interfaces and undergo absorption within the layers. We refer to the parameterization of the transmission and reflection as an interface model. In what follows we discuss an interface model that is based on scalar scattering theory.

According to nonparaxial scalar scattering theory [15, 16], the diffracted radiance of wavelength λ in direction cosine space is given by

$$L(\alpha, \beta - \beta_0) = \frac{\lambda^2}{A_s} |\mathscr{F}\{U_0(\hat{x}, \hat{y}) \exp(i2\pi\beta_0\hat{y})\}|^2. \tag{1}$$

A_s denotes the aperture area. The pupil function U_0 represents the phase variations acquired by a plane wave traversing the interface. The term $\exp(i2\pi\beta_0\hat{y})$ represents the phase variation introduced by oblique incidence. The angle resolved scattering (ARS) can then be obtained by [14]

$$\text{ARS}(\phi, \theta) = \cos(\theta) \cdot L(\alpha, \beta) \cdot A_s. \tag{2}$$

The coordinate transformation from direction cosine space (α, β) to spherical coordinates is given by $\alpha = \sin\theta \cdot \cos\phi$ and $\beta = \sin\theta \cdot \sin\phi$. The integration over the hemisphere is illustrated in Fig. 1. For non-planar surfaces the reflected light is not confined to the plane of incidence Γ_0 and the integration collects all light that is scattered into planes Γ_ϕ.

Thus, integration of the computed scattering intensity distributions, according to equation 2, over the hemisphere is used to construct the layer interface boundary conditions for our absorption model, where Fresnel's equations are used to ensure conservation of energy. Note that the terms angular intensity (AID) [6] and bidirectional scattering distribution function

#233350 - $15.00 USD Received 6 Feb 2015; revised 17 Mar 2015; accepted 18 Mar 2015; published 17 Apr 2015
(C) 2015 OSA

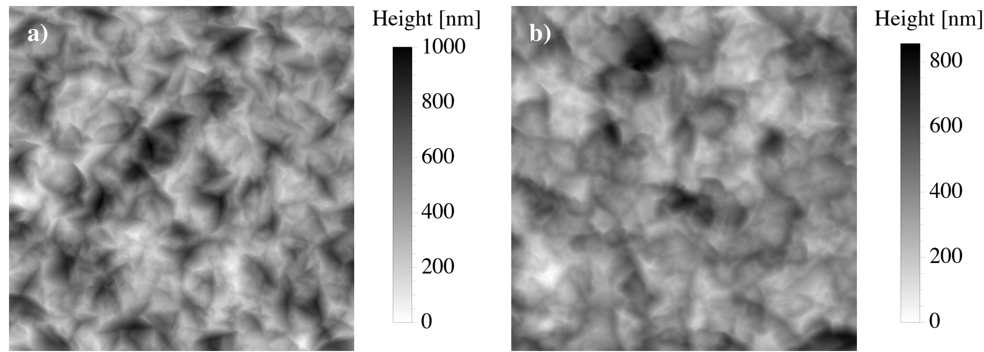

Fig. 2. Atomic force microscopy (AFM) measurements of the two analyzed ZnO substrates. The dimensions of the scans are 10 by 10 μm^2 and the root-mean-square (RMS) roughnesses of the substrates are 150 nm (a) and 120 nm (b).

(BSDF) [17, 18] are also used in the literature to denote the scattering intensity distributions. In non-paraxial scalar scattering theory the diffracted radiance is shift invariant in direction cosine space. This can be exploited in the computation of the angle resolved scattering (ARS) for different incidence angles as only a single Fourier transform is necessary for all incidence angles. Further, the hemispherical integration leads to a vast reduction of the degrees of freedom, allowing for an efficient numerical scheme.

Earlier contributions have already demonstrated that non-paraxial scalar scattering theory correctly reproduces measured ARS curves for normally incident light [14, 19]. Here we present experimental validation also for the case of oblique incidence. We analyze two ZnO transparent electrodes grown by low-pressure chemical vapor deposition. After deposition a plasma treatment is used to render the substrates suitable for the deposition of microcrystalline silicon. The resulting root-mean-square (RMS) roughnesses of the two substrates are 150 nm and 120 nm, see Fig. 2.

The texture information, as measured by AFM, enters the computation of the ARS via the pupil function U_0 (equation 1). The resulting diffracted radiance is illustrated in Fig. 3. The red circle denotes the unit circle where $\left(\alpha^2+\beta^2\right)=1$, only modes within are considered propagating. Oblique incidence, Fig. 3(b), leads to a shift of the radiance in direction cosine space, whereas the shape of the radiance stays the same. Note however, that this shifts some modes beyond the horizon (they are considered evanescent) and that the resulting radiance, and consequently also the ARS, is no longer statistically rotationally symmetric. As noted above, constructing the boundary conditions for our non-iterative ray-tracing requires integrating the computed radiance over spherical segments of the hemisphere, thus solid angles with equal polar angle. The blue circles in Fig. 3 illustrate such spherical segments.

In Fig. 4 we present measured and computed ARS curves for transmission trough the ZnO/air interface for the two substrates. Both normal and oblique incidence are shown, at a wavelength of 543 nm. For the measurement a detector scans the scattered transmission over all polar angles for one constant azimuth angle. The two ZnO substrates are deposited on glass and the incidence angle given in the figures refers to the angle in ZnO. For the rough substrate, Fig. 4(a), the incidence angle in air is 49°, corresponding to 26° (0.46 rad) in ZnO. For the less rough substrate, Fig. 4(b), the incidence angle in air is 40° corresponding to 21° (0.37 rad) in ZnO. The glass faces the light source. Note that in our home-built measurement setup the incidence angle is controlled by rotating the sample by hand and that we determine the incidence angle by locating the specular part of the transmission. Hence the small difference between the two oblique incidence angles. Given the large dynamic range of transmission intensities the

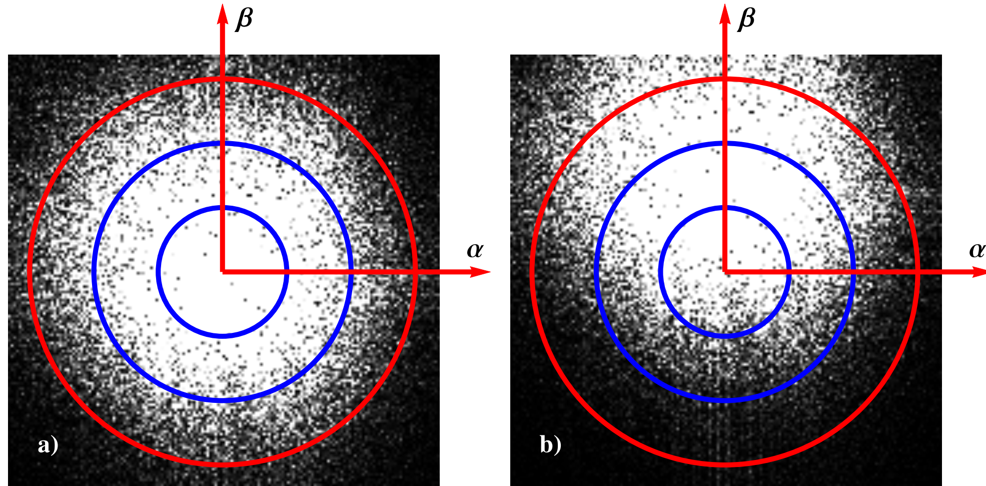

Fig. 3. Illustration of the computed diffracted radiance for scattering from the ZnO/silicon interface (RMS roughness 120 nm) into silicon. (a) Perpendicular incidence; (b) oblique incidence. The red circles denote $(\alpha^2+\beta^2)^{1/2}=1$, only modes within this unit circle are propagating.

computation reproduces all measurements very well. Only for angles far off from the specular direction in oblique incidence does the computation systematically underestimate the measurement. This limitation of the model can be understood by considering the approximation of the rough interface by a phase-screen of zero thickness [19].

3. Results

We apply our method to study the layer absorbances in microcrystalline silicon (μc-Si:H) solar cells with absorber thicknesses of 1 μm deposited on the two ZnO substrates. The solar cells have been presented in [7] and have the layer structure glass / ZnO (5 μm) / μc-Si:H (1 μm) / ZnO (5 μm) / white paste back reflector. Despite the large differences observed in the ARS, the two substrates lead only to slight differences in the EQE. In our model of the devices we use the measured texture information to simulate the light scattering at the ZnO front contact/silicon and at the ZnO back contact/siIicon interface. Hereby we carry out the ARS calculations for the material interface pairs ZnO/silicon instead of ZnO/air. In Fig. 5 we compare the measured external quantum efficiency (EQE) and reflection to the computed spectral layer absorption in the intrinsic layer (thus assuming ideal carrier collection) and reflection. For the EQE we do find an excellent agreement between measurement and simulation over the entire spectral range. The solar cell on the rough substrate, Fig. 5(a), shows slightly better light trapping with a measured photocurrent of 23.0 mA/cm^2 (simulated 23.8 mA/cm^2), compared to 21.9 mA/cm^2 (simulated 21.9 mA/cm^2) for the other substrate. With the assumption of Lambertian light trapping we find a photocurrent of 26.6 mA/cm^2. For the reflection we only find a good agreement in the spectral range up to about 800 nm. Most likely this overestimation is due to our use of Fresnel's equations in the normalization of the boundary conditions. The shaded areas in the figures represent the computed spectral parasitic absorption that can be quantified by an equivalent current density. We stress that these results are computed solely on the basis of the measured surface textures, the spectroscopic ellipsometry measurements of the materials and the layer thicknesses. In contrast to earlier reported methods we do not rely on measured reflection spectra and do not make any a priori assumptions about the degree of parasitic absorption. Further, our

#233350 - $15.00 USD Received 6 Feb 2015; revised 17 Mar 2015; accepted 18 Mar 2015; published 17 Apr 2015
(C) 2015 OSA

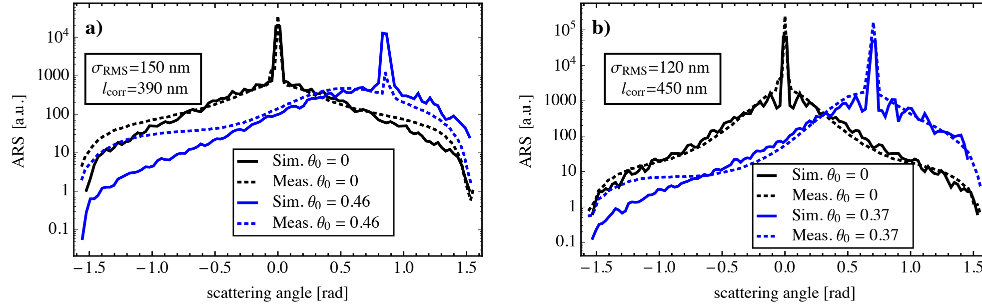

Fig. 4. Angular resolved transmission through the two ZnO surfaces: (a) $\sigma_{RMS} = 150\ nm$, (b) $\sigma_{RMS} = 120\ nm$ into air for monochromatic light with a wavelength of 543 nm at normal and oblique incidence. Solid lines represent calculations, dotted lines measurements. The inset gives the root-mean-square roughness and the correlation length of the two substrate textures.

method does not make any assumptions about the internal intensity distribution of the scattered light but computes the scattering for all internal propagation directions. As we show below, this allows for a direct comparison of the scattering structure to an ideal Lambertian scatterer.

We now turn to investigate further the internal light propagation, which ultimately determines the degree of light trapping. In the framework of statistical ray optics scattering is often described by ideal Lambertian scatterers. One thereby assumes that light propagating inside the absorber shows full randomization that is described by a Lambertian distribution. In our framework we compute the scattering based on the measured interface texture and the incidence angle not only for the first scattering event but also for all subsequent ones. In Fig. 6 we show the resulting azimuthally integrated ARS, labeled $\text{ARS}_{\bar{\phi}}$ for the two textures at a wavelength of 700 nm. $\text{ARS}_{\bar{\phi}}$ initial represents the transmission through the ZnO/silicon interface and $\text{ARS}_{\bar{\phi}}$ equilibrium the intensity distribution containing all propagating modes. By comparing with the thermodynamically optimal Lambertian distribution we can confirm that the rougher substrate is indeed closer to an ideal scatterer, corroborating the experimental finding. We note that the equilibrated $\text{ARS}_{\bar{\phi}}$ is indeed closer to a Lambertian, illustrating the (partial) randomization of the radiation. The capability of computing the internal intensity distributions

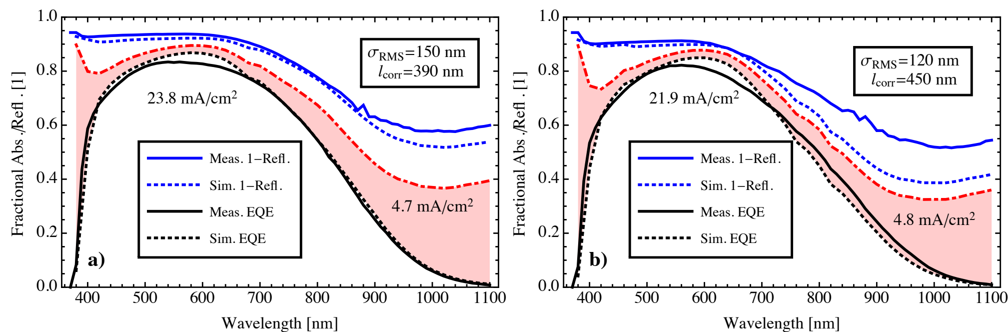

Fig. 5. EQE and 1-R curves for μc-Si solar cells deposited on the two substrates with intrinsic layer thicknesses of 1 μm. The dashed curves represent the calculations. The shaded area in the figures represents the parasitic absorption in the electrodes, quantified by an equivalent current. The inset gives the root-mean-square roughness and the correlation length of the two substrate textures. Also given are the computed photocurrents.

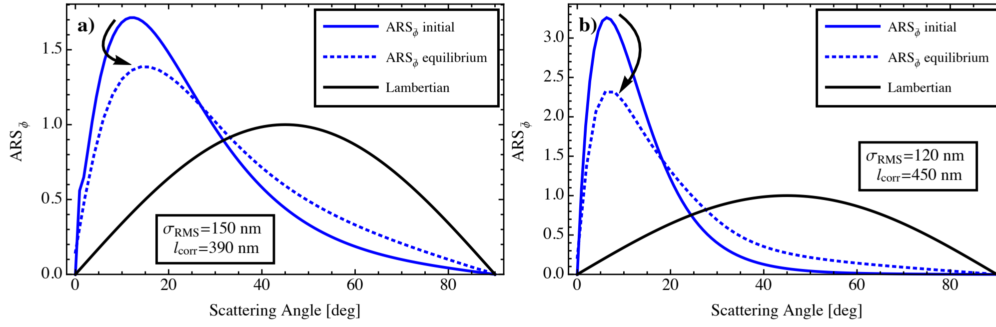

Fig. 6. ARS$_{\bar{\phi}}$ for a wavelength of 700 nm for the two substrates: (a) $\sigma_{RMS} = 150\ nm$, (b) $\sigma_{RMS} = 120\ nm$. The initial transmission into silicon (solid blue), the equilibrated distribution containing all propagating modes (dotted blue) and a Lambertian scatterer (solid black). The inset gives the root-mean-square roughness and the correlation length of the two substrate textures.

thus provides an experimentally unaccessible insight into the light trapping.

As we pointed out above, the light trapping will not only determine the photocurrent but also the parasitic absorption. We can use our model to illustrate this interdependency: we compute the photocurrent in a microcrystalline silicon solar cell where we parametrize the specularity of the light scattering at the textured interfaces by the Phong model [20]. For normal incidence the Phong model can be written as $ARS(\phi,\theta) = \cos(\theta)^l$, where l denotes the Phong factor. For normal incidence and a Phong factor of 1 this produces a Lambertian distribution. Note however, that the scattering intensity distributions according to this model do depend on the incidence angle. Phong factors above 1 produce more specular, factors below 1 broader intensity distributions. In the limit of very large Phong factors, the distribution becomes purely specular. In Fig. 7 we present the computed photocurrent for Phong factors varying between 0.1 and 100 and three different electrode thicknesses. For an electrode thickness of 2 μm we find an optimal value of 1.5 for the Phong factor, whereas for an electrode thickness of 8 μm 0.1 is optimal. Inspection of the internal ARS$_{\bar{\phi}}$, as shown in Fig. 7(b) for a wavelength of 700 nm and Phong factor 1.5, confirms that such a scattering behavior does indeed lead to almost ideal internal light scattering.

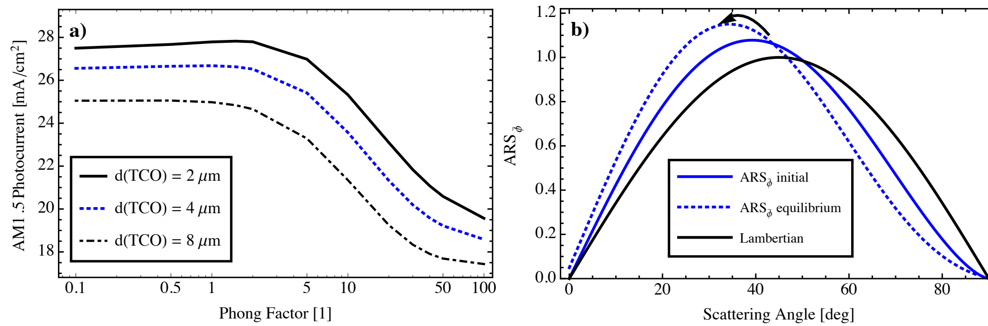

Fig. 7. (a) Parametric variation of the specularity of the scattered light, parametrized by the Phong Factor. (b) ARS$_{\bar{\phi}}$ for a wavelength of 700 nm for Phong factor 1.5. The initial transmission into silicon (solid blue), the equilibrated distribution containing all propagating modes (dotted blue) and a Lambertian scatterer (solid black).

#233350 - $15.00 USD Received 6 Feb 2015; revised 17 Mar 2015; accepted 18 Mar 2015; published 17 Apr 2015
(C) 2015 OSA

4. Conclusions

We have extended our optical solar cell model [12] to directly account for textured layer interfaces that we tackle with non-paraxial scalar scattering theory. This ab initio approach is amenable to a purely experimental input without simplifying assumptions and allows for computationally efficient simulations compared to more brute force full-wave simulation methods. Very good agreement between simulated active layer absorption spectra and measured EQE spectra was found for microcrystalline silicon solar cells deposited on a rough ($\sigma_{RMS} = 150\ nm$) and a slightly less rough ($\sigma_{RMS} = 120\ nm$) ZnO transparent electrode. The presented method is now made available in the optoelectronic simulation software package *setfos* [17]. Several features of our method distinguish it from earlier presented methods: we compute all internal scattering distributions based on measured surface textures rather than making a priori assumptions about them; the spectral parasitic absorption is an output of our model rather than being deduced from separate substrate measurements; we can extract the equilibrated internal intensity distributions that are ultimately decisive for the light trapping. Meanwhile our modeling approach has also proven very useful for simulating large area emissive thin-film OLEDs with interface textures [18].

Acknowledgments

Financial support by Swiss Electric Research and the Swiss Competence Center for Energy and Mobility in the framework of the projects DURSOL and CONNECT-PV is gratefully acknowledged.